High-Q MEMS for Wireless Integrated Circuits

Victor M. Lubecke, Bradley P. Barber, Linus A. Fetter

Abstract - **While integration technology has steadily improved size and performance for wireless baseband circuitry, quality factor and frequency limitations still limit RF front-end circuitry to many large discrete components. Integration solutions for two such RF components are described here. Silicon MEMS techniques are used to create self-assembled inductors with reduced losses and improved high frequency characteristics compared to conventional integrated inductors. The same technology is used to demonstrate variable inductors. Filter technology based on micromachined acoustic wave resonators is also presented, offering reduced size over conventional resonators as well as an integration path.**

Index Terms **- MEMS, RFIC, BAW, micromechanical, acoustic, resonator, inductor.**

I. INTRODUCTION

THE growing demand for smaller and more capable mobile telephones and other wireless communications terminals has created a pressing need for extremely compact and power efficient radio circuitry. While the size, performance, and cost benefits of integration technology has been widely exploited in baseband circuitry for these products, RF front-end circuitry has remained heavily dependent on large discrete passive components, particularly for resonant functions where inefficient integrated components would seriously degrade performance [1]. These circuit applications include resonators for low phase-noise voltage controlled oscillators (VCO's), filter components, and reactive impedance matching elements.

Many resonator functions can be performed with conventional inductor-capacitor (L-C) circuits. These are passive components that store energy in localized electromagnetic fields. However, integrated-circuit versions of these components, particularly inductors, are generally severely limited by parasitic losses. In order to minimize ohmic loss, thin-film spiral inductors are invariably large, and thus account for the majority of circuit area in typical RF integrated circuits (RFIC's). Furthermore, when combined with the high conductivity of RFIC substrates, this broad, flat geometry results in a large parasitic capacitance that limits both quality factor (Q), and self-resonance frequency (SRF). Loss reduction techniques such as local substrate removal and vertical construction can help, but not without imposing fabrication and compatibility issues [2,3]. Through micro-electromechanical systems (MEMS) techniques, inductors can be made which minimize this loss mechanism through three-dimensional self-assembly [1]. The technique also allows for the creation of variable inductors that are not subject to the same constraints as those achieved through active circuitry [4,5]. Various MEMS inductors with Q values greater than 13 and inductance variations exceeding 18% are presented, with clear potential for even better performance. These inductors are well suited to integration in RFIC VCO's and low noise amplifiers (LNA's) [6].

V. M. Lubecke is with Bell Laboratories, Lucent Technologies, Murray Hill, NJ, 07974 USA, (e-mail: lubecke@lucent.com).

B. P. Barber, and L. A. Fetter are with Agere Systems, Murray Hill, NJ, 07974 USA, (e-mail: bbarber@agere.com, lfett@agere.com).

Single element resonators are attractive for wireless handset front-end duplex filters. Often discrete ceramic resonators are used for high Q values, with the caveat of large size. Surface acoustic wave (SAW) filters offer a more compact option, yet typically provide reduced performance. Alternatively, bulk acoustic wave (BAW) resonators can be used for many RF filter and oscillator applications. In bulk-mode acoustic filters, energy is stored as both electromagnetic and mechanical energy through piezoelectric coupling. Because the velocity of sound in the piezoelectric layer is much smaller than that of light, these devices can be much smaller than conventional high performance cavity resonators while maintaining improved power handling and frequency capability over SAW devices. Various BAW resonators and filters are described, demonstrating excellent Q values up to 1000. These BAW resonator technologies are also well suited for integration with RFIC's [7].

II. MEMS RF INDUCTORS

When placed on a low-resistivity substrate, planar inductor geometries present both a desired inductance and a parasitic capacitance. Reducing the size of the conducting elements brings about a reduction in parasitic capacitance, but also increases the resistive loss. The approach presented here for improving this situation involves lifting the structure off the substrate plane to reduce the capacitance without increasing the resistance. The inductors assemble by means of an interlayer stress that causes portions of the inductor to bend away from the substrate in a controllable manner [8,9], as shown in Fig. 1(a). The fabrication process involves conventional silicon surface micromachining techniques that allow batch processing, as shown in Fig. 1(b), and can potentially be integrated with electronic circuits.

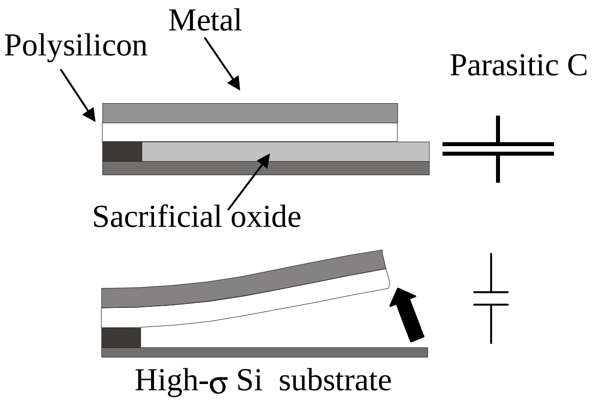

(a)

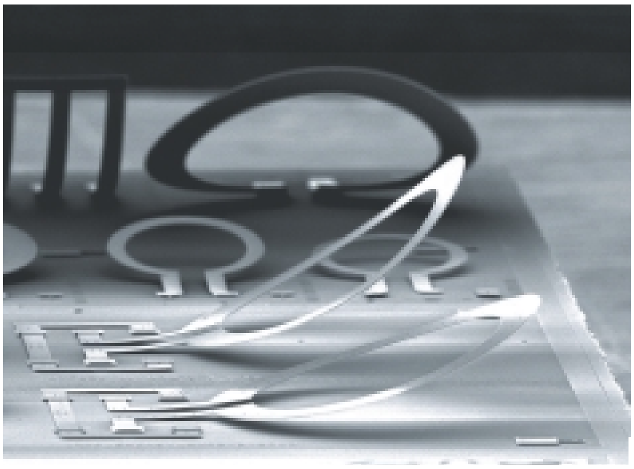

(b)

Fig. 1. Self-assembling inductor. When released, interlayer stress causes the inductors to bend away from the substrate and reduce parasitic capacitance (a). SEM micrograph shows various inductors simultaneously assembled (b).

A. Design and Fabrication

A high performance variable inductor can be formed by creating a structure that remains sufficiently isolated from the substrate at all operating temperatures, yet incorporates mutually coupled current-carrying members that move with respect to each other with varying temperature, thus affecting the mutual component of the total inductance. The temperature variations needed to actuate such a structure can be environmental, or localized joule heating effects induced by an applied DC current [1]. One such variable inductor is shown in Fig. 2. The inductor consists of two loops that assemble themselves above the substrate, with a relative angle between them that can be thermally controlled. The differential motion results from a cross-member corrugation structure in the inner loop that causes it to bend with temperature at a different rate than the outer loop. The conductors were ~50μm wide, separated by a ~20-μm gap, and the longer loop was about 1200μm long. The pitch between anchor pads was 150μm.

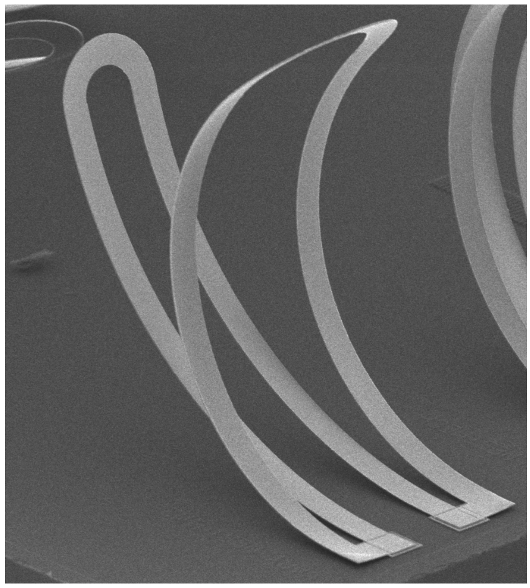

Fig. 2. Self-assembling variable inductor. When heated, mutually coupled loops (about 1200μm long) bend at different rates to allow controlled variation of inductance.

The same self-assembly technique has been used to make fixed value inductors with high Q and SRF values [6]. Limiting parasitics for these structures occur near the anchor pads where the loop structure remains close and roughly parallel to the substrate, and the performance for these inductors is subject to change when exposed to physical shock and thermal variations that cause the structure to flatten towards the substrate. An improved variation on this design shown in Fig. 3. This hairpin inductor is attached to the substrate by hinges rather than anchor pads and warping elements are used to assemble the inductor into a locking semi-vertical position that changes very little with subsequent temperature changes. The hinges can be further fixed in place by electroplating the structure, which can also create a dependable ohmic connection to a circuit. The conductors were ~50μm wide, and the loops about 1200μm long. The pitch between attachment points was 150μm.

Fabrication of the fixed and variable inductors was performed through photolithographic techniques. The structures were formed as a Cr-Au layer (0.5μm+) over a polysilicon layer (1.5μm), patterned on a sacrificial oxide layer (2μm) over the substrate, with a final etch-release/self-assembly step to achieve the desired three-dimensional structures [6]. The resulting (non-hinged) structures were resilient, springing back after mechanical probing, and the designs were repeatable.

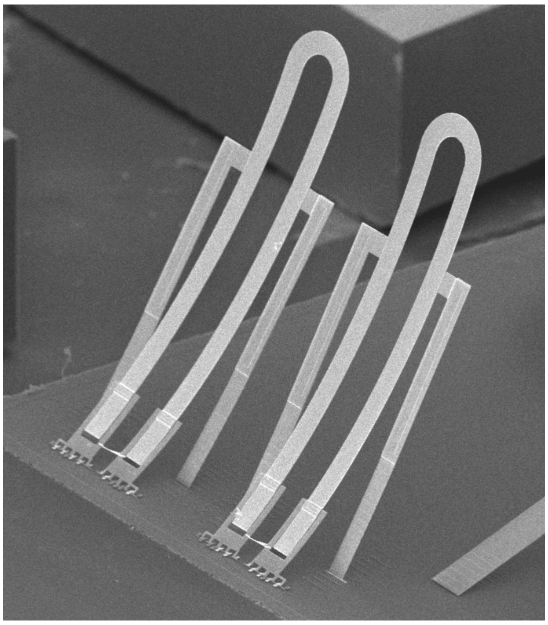

Fig. 3. Self-assembling fixed-value inductors. Interlayer stress causes the legs to bend, raising the hinged hairpin-shaped structure (about 1200μm long) to a locking position for improved Q, SRF, and thermal/mechanical stability.

Fabrication was carried out using the Cronos Multi-User MEMS process (MUMPS) [10]. While this process was suitable for demonstrating the inductor concept, it imposes unnecessary limits on inductor performance. The substrate has higher conductivity (1 Ω-cm) than needed for an RFIC (up to 10 Ω-cm), which results in lower Q. Another significant limitation is the single metal layer in this process, which is too thin to minimize ohmic losses (less than one skin depth), and limits inductance to low values by restricting designs to a single turn (no bridge layer). The process however, is convenient, widely used, and allows for the demonstration of an effective technique for fabricating MEMS-first integrated RF inductors. The process provides a reasonable representation of RFIC demands, provides the basic features of promising embedded MEMS approaches [11], and can be readily modified to remove the aforementioned limitations.

B. Performance

Various self-assembling inductors were fabricated and their scattering parameters measured using a Cascade-Microtech Microchamber probe station with ambient temperature control, and an HP 8510B network analyzer. The performance of a variable inductor is shown in Fig. 4. Frequency-swept measurements were made for temperatures ranging from 25˚C to 200˚C. At room temperature, the outer loop of the inductor stood at an angle of about 45 degrees, and the inner loop was bent even further (see Fig. 2). As temperature was increased, both loops began to straighten out and flatten towards the substrate at different rates. In this case, neither loop went totally flat against the substrate, even at 200˚C. In the vicinity of 4 GHz, Q values remained fairly stable around 5 (<10% variation), while inductance values varied from 0.67 nH to 0.82 nH, greater than 18% (22% referenced to the heated extreme). The values were repeatable as the temperature was cycled. The ambient temperature for the inductors was varied here, but it is also possible to achieve this effect by directly heating only the inductor structure by applying a DC current.

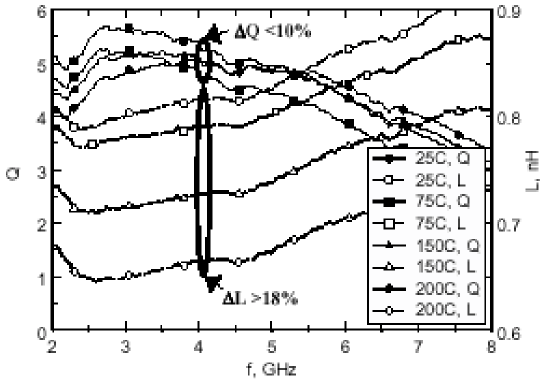

Fig. 4. Performance of a self-assembling variable inductor. Inductance varies as loops deform with temperature. Q values remained fairly stable around 5 (<10% variation), while inductance values varied over an 18% (22% referenced to the heated extreme) range.

A comparison of two similar fixed-value inductors is shown in Fig. 5. Both were hairpin-shaped, but one was a simple warping structure attached to the substrate with flat anchor pads (similar to the inner loop in Fig. 2), while the other was attached with hinges as previously described (see Fig. 3). Measured inductance values were very similar for both (~1 nH), with a slightly higher value for the simple inductor due to the extra length of the anchor pads. At very low frequencies, Q values were similar, as the thin metal was the limiting factor in both cases. At higher frequencies though, the Q value was greatly improved for the hinged inductor, in excess of 13. Furthermore, very little change in inductance was observed for the hinged inductor at varying temperatures.

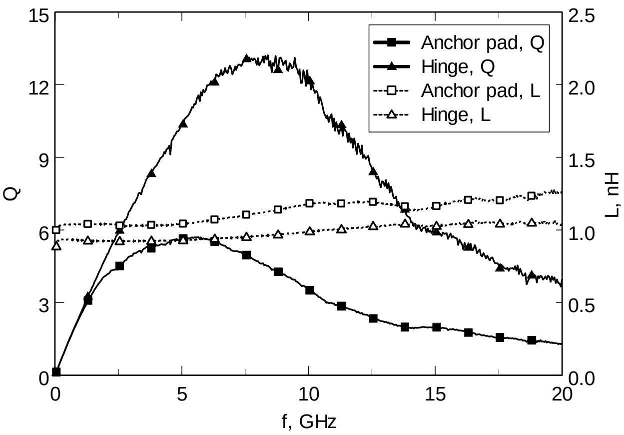

Fig. 5. Self-assembling fixed-value inductors. Hinged structure shows improved Q over warped structure, and can be further improved with thicker metal.

While a simple hairpin design was useful for demonstrating the variations in Q and inductance described above, the absolute performance for this structure was not ideal. Even with only thin metal, wider inductors with a more circular or triangular shape have demonstrated Q values that rise more quickly with frequency and peak at levels greater than twice that of the hairpin. These structures could also be adapted in the same manner as the hairpin inductors described here. Previous analysis indicates that increasing the metal thickness for these inductors to about two skin depths (3µm at 2 GHz) should result in peak Q values greater than 20 [1]. An additional set of metal and sacrificial layers would also be useful for creating a conducting bridge or underpass, which would allow for the creation of multiple turn inductors with much higher inductance. These improvements could be easily achieved through custom MEMS processing, or post-processing depositions on a foundry processed wafer.

Wire loop model simulations for variable inductors using Fasthenry [12] field solver software suggest the range of inductance variation for the two-loop configuration can be enhanced, by increasing the coupling between the loops. Figures 6 and 7 illustrate how reducing the gap between inner and outer loops (Fig. 6) from 25 µm to 5µm results in the maximum inductance variation changing from of 27% (37% referred to the alternate extreme) to about 34% (51%), when the angle between the loops varies from 0 to 90 degrees (Fig. 7). Substrate coupling was neglected for these simulations as both loops maintain a position above the substrate for the majority of travel.

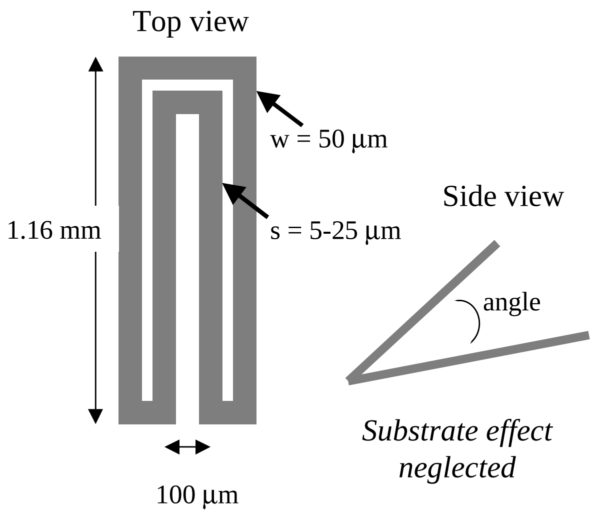

Fig. 6. Conceptual illustration of self-assembling variable inductor.

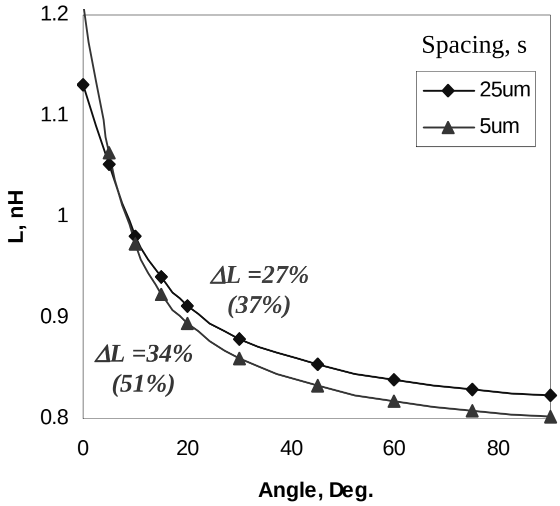

Fig. 7. Variable inductor simulation. Decreasing the gap between loops increases the maximum mutual coupling and can thus increase the range of inductance variation.

III. BULK ACOUSTIC WAVE RESONATORS

One of the most promising technologies for high-Q integrated wireless filters is based on the micromachining of piezoelectric films to form bulk acoustic wave resonators. A combination of sharp cut-off characteristics, compact size, and practical fabrication makes these resonators attractive for demanding applications, such as wireless PCS duplex filters used to separate closely spaced transmit and receive frequencies [13]. While ceramic resonator technology can meet challenging PCS specifications, smaller integrated solutions would allow for smaller and less expensive mobile handsets. Acoustic wave resonator technology can be used to this end. One key advantage in fabricating BAW resonators over SAW devices is that the critical frequency dependent dimensions are the thickness of the films, rather than lateral dimensions of planar lithography. Figure 7 illustrates this difference [14].

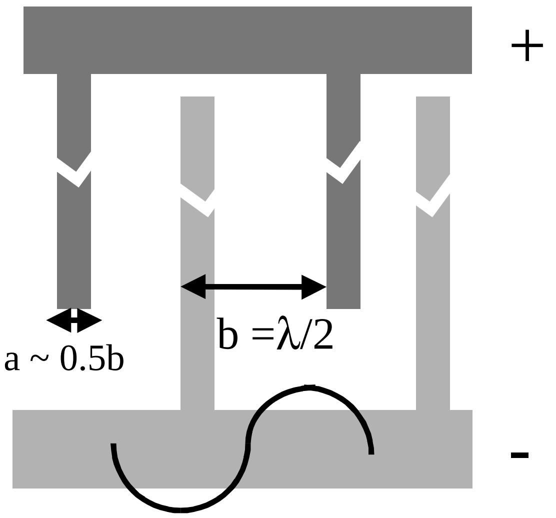

SAW Device

(a)

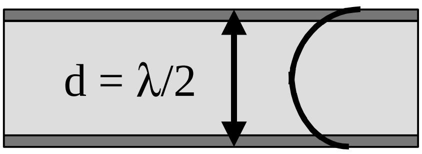

BAW Device

(b)

Fig. 7. Acoustic wave resonators. SAW devices depend on planar lithographic dimensions that become small with increasing frequency and are thus more difficult to control than the film thickness parameters of a BAW device.

A. Resonator Design and Fabrication

Two methods for the construction of such resonators are illustrated in Figures 8 and 9. Figure 8(a) shows a membrane based resonator, with the piezoelectric film suspended over a cavity etched in the substrate [15]. The air-piezoelectric film boundary forms an optimum impedance discontinuity. An SEM photograph of an array of front-side etched membrane resonators is shown in Fig. 8(b). Figure 9(a) shows an alternative technique, with a piezoelectric film over an acoustic mirror made of alternating dielectrics layers [16]. The dielectric Bragg stack forms a large impedance discontinuity at the design frequency. Figure 9(b) shows an SEM photograph of an acoustic mirror type resonator made using layers of silicon dioxide and silicon nitride.

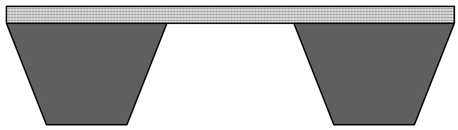

Etched Membrane

(a)

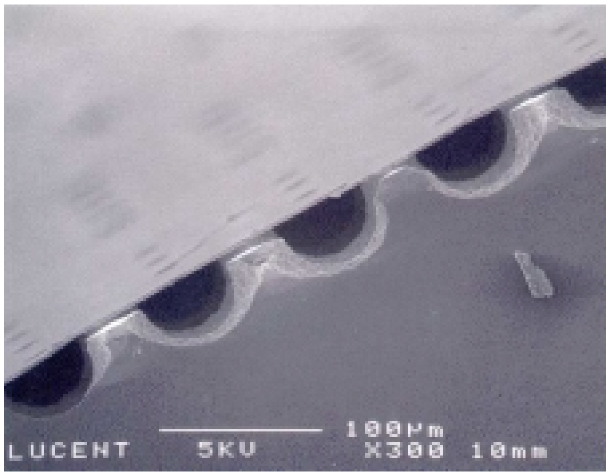

(b)

Fig. 8. Concept (a) and side view SEM photograph (b) of a membrane-type BAW resonator. The substrate is etched from beneath the piezoelectric film to optimize the impedance discontinuity on both sides.

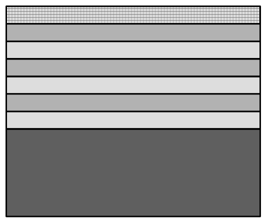

Bragg Stack

(a)

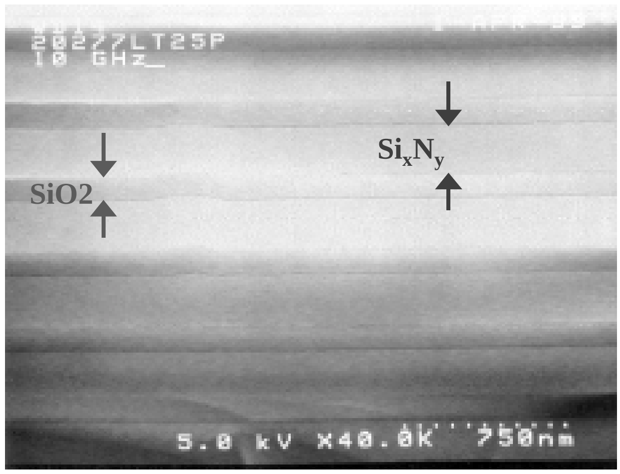

(a)

Fig. 9. Concept (a) and side view SEM photograph (b) of an acoustic mirror type BAW resonator. A Bragg stack formed by alternating layers of different dielectrics creates a large impedance discontinuity below the piezoelectric film at the design frequency.

B. Performance and Circuit Considerations

The electrical response of a BAW resonator has a sharp impedance minimum (zero) near a high impedance peak (pole). The speed of sound and thickness of the piezoelectric film (AlN here) determine the zero's frequency, and the zero-pole spacing is set by the electromechanical coupling k2. The complex mode structures of a BAW film near resonance is illustrated in the sub-angstrom interferometric measurements plotted in Fig. 10 [14]. The impedance characteristics for a classic "T" cell structure is shown in Fig. 11, illustrating how series and shunt elements of slightly differing frequencies can be used to form a band pass filter.

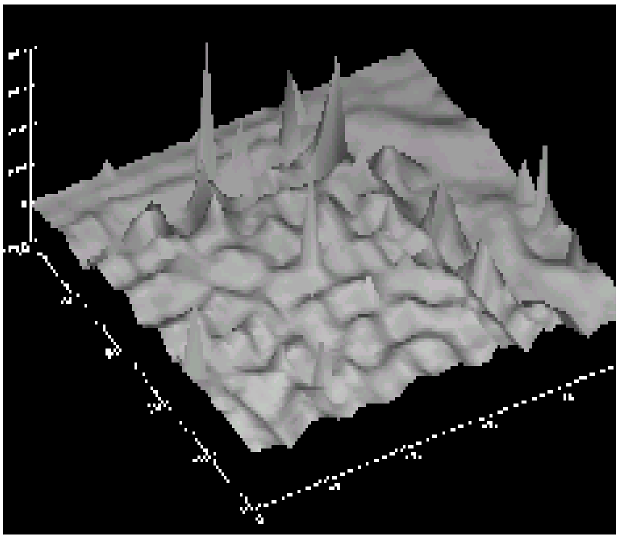

Fig. 10: Plot of scanning optical interferometer measurements with horizontal resolution ≈ spot size ≈ 1 µm, and vertical resolution: $10^{-6}\,\lambda_{op} \approx 0.01$ Å

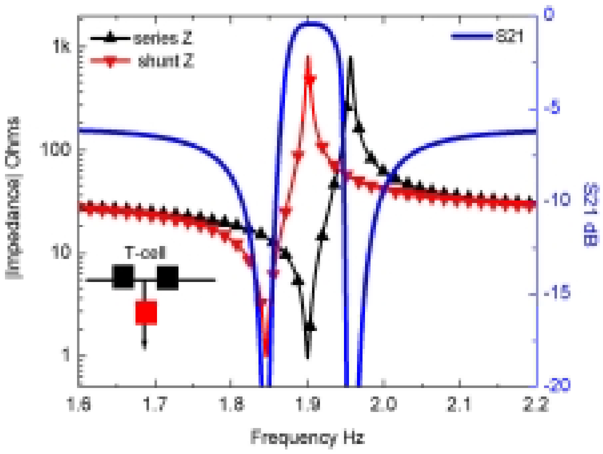

Fig. 11. Resonator impedance and transmission from a T-cell configuration. Series and shunt elements of similar frequency are combined to form a steep cut-off band pass filter.

From Fig. 11 it is evident that a wider separation between zero and pole allows for wider bandwidth (BW) filters. However, material constraints limit the available resonator range and thus additional circuit elements are sometimes required to achieve a satisfactory filter. For example, to cover the PCS band with a filter using an acoustic-mirror based filter, external series inductors can be required. (SiO2 & AlN Bragg stack) under an AlN piezoelectric film, external inductors would be required in series with the BAW resonators for full coverage of the frequency range [7].

One such filter was constructed using an SiO2/AlN Bragg stack under an AlN piezoelectric film and external series inductors. The performance is shown in Fig.12.

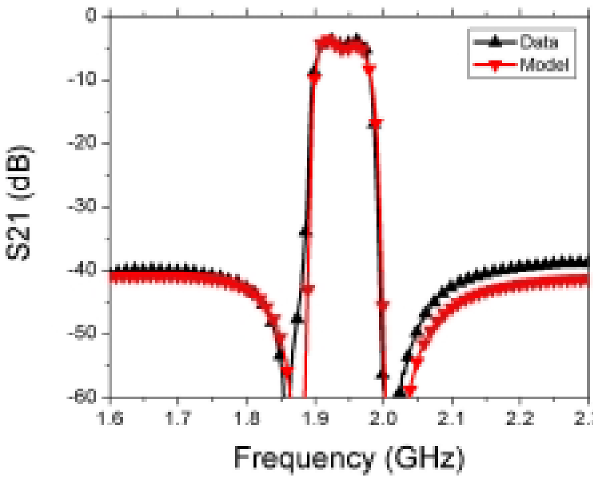

Fig.12. PCS BAW filter made on a acoustic mirror using series inductors to widen the resonators' bandwidth.

The external inductors for such filters are on the order of 1 nH, which means that integration and size advantages can be lost unless high-Q integrated inductors can be used. While more difficult to construct, membrane based resonators can achieve a typical 50% increase in pole zero separation without inductors. Filters for GSM applications, with their large required bandwidth, can thus be constructed without additional passive elements. Other RF bands, e.g. 5.2 GHz LAN, may require both membranes and inductors to cover the bandwidth. A micrograph of an optimized membrane filter is shown in Figure 13. The front-side etch holes evident around the resonator are used to remove a sacrificial layer and free the membrane. The devices are proof of principle, but improvements in Q and spectrum clarity must be achieved before our BAW devices surpass their SAW competition on specifications alone.

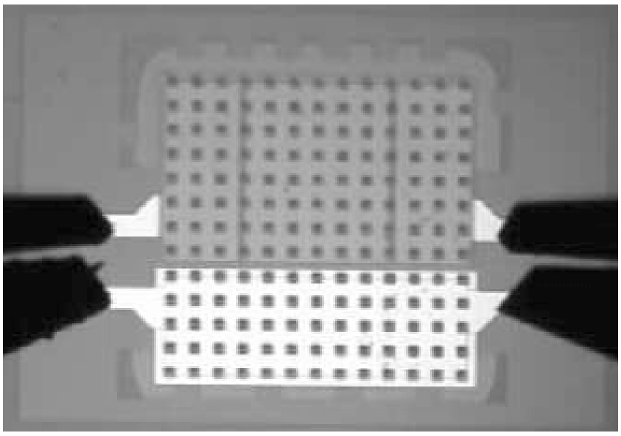

Fig. 13. Micrograph of a membrane based BAW filter.

IV. Conclusions

Two important wireless resonator technologies have been presented. MEMS RF inductors can provide improved Q and SRF over conventional RFIC inductors, without sacrificing the benefits of integration. Fixed value thin metal inductors were demonstrated with Q values better than 13, with the potential for Q's in the 20's. Variable inductors were demonstrated with a near 20% change in inductance, with the potential for variations on the order of 50%. Bulk acoustic wave resonators were also examined for use in wireless filter applications, where they offer reduced size over ceramic resonators and improved high-power and high-frequency response over SAW devices. Simple acoustic mirror BAW devices offer good resonator characteristics with bandwidth that can be improved with external inductors. Membrane devices offer improved stand-alone bandwidth, with the potential to extend the technology to higher frequency wireless applications.

V. Acknowledgments

The authors wish to acknowledge the support of Lucent Technologies and Agere Systems (formerly the Microelectronics division of Lucent Technologies). We would also like to thank K. Grenier E. Chan, J. Lin, O. Boric-Lubecke, P. Gammel, and L. Manzione for their support.

References

[1] P.L. Gammel, B.P. Barber, V.M. Lubecke, N. Belk, M.R. Frei, "Design, Test and Simulation of Self-Assemblied, Micromachined RF Inductors", *SPIE Symposium on Design, Test, and Microfabrication of MEMS and MOEMS*, pp 582-591, March 1999.

[2] C.-Y. Chi and G.M. Rebiez, "Planar Microwave and Millimeter-wave Lumped Elements and Coupled-line Filters Using Micromachining Techniques", *IEEE Trans. Microwave Theory. Tech.*, vol. MTT-43, pp. 730-738, April 1995.

[3] D. J. Young, V. Malba, J.-J. Ou, A.F. Bernhardt, and B.E. Boser, "Monolithic High-performance Three-dimensional Coil Inductors for Wireless Communication Applications," *Technical Digest, IEEE Intl. Electron Devices Meeting*, Washington, D. C., pp. 67-70, Dec. 8-11, 1997.

[4] Shifang Zhou, Xi-Qing Sun and William N Carr, "A Monolithic Variable Inductor Network Using Microrelays with Combined Thermal and Electrostatic Actuation", *Jrnl. of Micromechanics and Microengineering*, vol.9, no.1, pp.45-50, March 1999.

[5] S. Hara and T. Tokumitsu, "Monolithic Microwave Active Inductors and their Applications", *IEEE International Symposium on Circuits and Systems*, pp. 1857-1860, June 1991.

[6] V. Lubecke, B. Barber, E. Chan, D. Lopez, and P. Gammel., "Self-Assembling MEMS Variable and Fixed RF Inductors," *Proc. of the Asia Pacific Microwave Conference (APMC)*, Sydney Australia, Dec. 2000.

[7] K. Grenier, B. Barber, V. Lubecke, M. Zierdt, H. Safar, P. Pons, and P. Gammel, "Integrated RF MEMS for Single Chip Radio," *Transducers digest*, Munich, Germany, May 2001.

[8] W. Cowan, V. Bright, V, A. Elvin, D. Koester, "Modeling of Stress induced curvature in surface micromachined devices," *SPIE Symp & Education Prog. on Micromachining and Microfabrication*, pp.56-67, 1997.

[9] V. Aksyuk, B.P. Barber, C.R. Giles, R. Ruel, L. Stultz, D.J. Bishop, "Low Insertion Loss Packaged and Fiber-Connectorized Si Surface-Micromachined Reflective Optical Switch," *Proc. 1998 Solid State Sensor and Actuator Workshop*, Hilton Head pp. 79-82.

[10] D. Koester, R. Majedevan, A. Shishkoff, K. Marcus, "Multi-user MEMS Process (MUMPS) Introduction and Design Rules," Rev. 4 7/15/96 MCNC (CRONOS) MEMS Technology Application Center, Research Triangle Park, NC 27709.

[11] J. Smith, "Embedded Micromechanical devices for the Monolithic Integration of MEMS with CMOS", *Proc. IEDM ' 95*, pp. 609-612, 1995.

[12] Fasthenry User's Guide, version 3.0, M. Kamon, L. M. Silveira, C. Smithhisler, J. White, Massachusetts Institute of Technology, Cambridge, MA, 11 November 1996. Fasthenry is an inductance extraction program that computes the complex frequency-dependent admittance matrix under the magnetoquasistatic approximation.

[13] P. Bradley, R. Ruby, J. Larson, Y. Oshmyansky, and D. Figuerdo, "A Film Bulk Acoustic Resonator (FBAR) Duplexer for USPCS Handset Applications," *IEEE MTT-S Int. Microwave Sym. Dig.*, May 2000.

[14] B. Barber, "Thin-Film Bulk Acoustic Wave Devices for RF Applications," presented at Sarnoff 2000, NJ March 2000.

[15] R. Ruby et al. "PCS 1900MHz duplexer using thin film bulk acoustic resonators (FBARs)", Elec. Lett. Vol. 35, No 10, pp794-795, May 1999

[16] KM. Lakin et al. "Solidly Mounted Resonators and Filters" 1995 IEEE Ultrasonics Symp, pp 905-908